Temperature Dependence of Electrical Transport in a Pressure-Sensitive Nanocomposite

Alexander J. Webb, David Bloor, Marek Szablewski and Del Atkinson.*

Department of Physics, Durham University, South Road, Durham, DH1 3LE, UK

Abstract

Printed nanocomposites are of significant applications potential in numerous technologies, such as touch-sensitive sensors and surfaces. Here, temperature dependent electrical transport measurements were undertaken on a recently developed screen-printed, multi-component, nanocomposite ink to develop a detailed understanding of the electrical transport mechanisms. A theoretical model combining contributions from linear percolative conduction, and non-linear conduction attributed to field-assisted quantum tunneling, successfully describes the temperature dependent conduction observed.

Keywords: Nanocomposite, field emission, touch sensitivity, temperature dependence

Introduction

Composite materials that are electrically conductive[1] have been actively researched[2] and developed for applications for more than half a century[3]. In bulk form, these materials typically consist of electrically conducting filler particles dispersed in an insulating matrix. Filler particle

materials are diverse and commonly include graphite[4], carbon black, and metal powders of varying size and shape[5], and more recently carbon nanotubes[6] and graphene[7,8]. The insulating matrix materials are equally varied, with a range of polymeric materials[9,10,11] and even cement[12] utilized. Previously, the electrical conduction of these composites has been described as a function of the filler particle loading using phenomenological percolation and effective media theories[13,14]. At low filler particle fractions, these composites exhibit electrical conductivity close to that of the insulating matrix material[15]. The conductivity remains low with increasing particle content until the filler fraction reaches the *percolation threshold*. The threshold is a critical particulate concentration above which networks of direct electrical connections form between the filler particles that bridge the composite material such that the composite becomes electrically conducting[16].

Quantum tunneling has been suggested as a conduction mechanism within some composite systems[17,18], leading to the recognition of the potential significance of field-assisted quantum tunneling mechanisms in some composite materials[19]. Tunneling processes may occur in composites comprising filler particles in close proximity, but not in direct contact, and with nanoscale features that act to enhance local electric fields[19]. Such systems may be modeled as a combination of ohmic connections between filler particles in physical contact and field-assisted tunneling between separated filler particles and/or clusters of filler particles[20]. Composites with a particulate filler fraction close to the percolation threshold can be sensitive to finger-touch pressure, where compression forces the particles into closer proximity or into direct contact, transforming the composite from electrically insulating to a conducting state.

Touch-sensitive, electrically-conducting composites are of growing applications importance for touch sensitive interfaces. Recently, a novel nanocomposite ink with pressure-sensitive electrical

conductivity functionality was developed that can be used as a component in printed electronics manufacturing processes[21]. The structure and pressure-sensitivity of this ink was described and the analysis of room temperature electrical measurements suggested tunneling conduction was present[21]. This paper describes a detailed temperature and pressure investigation of the electrical conductivity behavior of this nanocomposite functional ink. This new experimental work details the temperature dependent electrical behavior which is relevant to both functional applications and provides a deeper understanding of the conduction processes that give rise to the pressure sensitivity of the electrical transport in this complex nanocomposite system.

Experimental Method

The nanocomposite ink in this study comprises commercially obtained nanoparticles at quantities above the percolation threshold, typically a concentration of the order of tens of percent, and base polymer ink. One "batch" contained 37.8 g Ishihara FT-2000 titanium dioxide needles (approximately 1.6 μm by 100 nm) with a semiconducting antimony-doped tin oxide surface coating (these will be referred to as TiO_2 needles henceforth), and 83.4 g Kronos Type 1080 electrically insulating, approximately spherical (diameter of around 200 nm on average) titanium dioxide nanoparticles (referred to as TiO_2 nanoparticles from here on out). It is worth noting that, while the TiO_2 needles are technically wide band-gap semiconductors, the antimony-doped tin oxide layer is conductive enough to regard the needles as good electrical conductors. The particles are dispersed in a conventional solvent based, commercially available, electrically insulating, flowing polyvinyl resin base ink (Polyplast Type PY383), as binder (73.5 g of PY383 and 55.3 g of Polyplast ZV545 solvent)[22]. The nanoparticles were produced by chemical synthesis methods; the authors refer the readers to the relevant patents for further details[23,24,25].

Titanium Dioxide has a melting point of 1843 °C and a thermal expansion coefficient of 9 x 10^{-6} K^{-1}, while the polymer base resin PY383 has a melting point of 158 °C. Here, the three constituents were mechanically blended, using a Dispermat VMA-Getzmann Model D-51580 bead mill (rotating at 4000 rpm) loaded with 80cc 0.8-1.0 mm beads. The blend was injected through the mill by a Dispermat SL at 0.7 mls^{-1}. Once a homogeneous suspension was obtained the resulting ink was screen-printed to manufacture test device structures, as shown in figure 1(a). A semi-automatic, manual load, flat-bed screen-printer was utilized to manufacture test structures. The test devices were printed onto an electrically insulating ceramic *macor* substrate with pre-prepared electrodes, chosen for its high temperature stability and negligible thermal expansion coefficient (9 x 10^{-8} K^{-1}). The printing process involved preparing a stencil, using computer aided design (CAD) and a laser cutter to produce the image mask. The stencil was then fixed to the printing screen; a woven mesh. The nanocomposite ink was poured onto the screen, after which a rubber squeegee was automatically pressed onto and across the entire screen, pushing the ink through the mesh and onto the substrate in accordance with the image negative mask. An ink layer of thickness 2 to 5 μm was printed onto the *macor* substrate. Post printing, the ink was dried in a furnace at 90 °C for 30 minutes to drive off solvents. The electrodes were deposited on to the ceramic substrates by thermal evaporation comprising a 2 nm chromium adhesive layer, a 150 nm copper conduction layer, and a 50 nm capping layer of gold. A single layer of the nanocomposite ink was screen-printed directly on to this electrode, as indicated in figure 1(b).

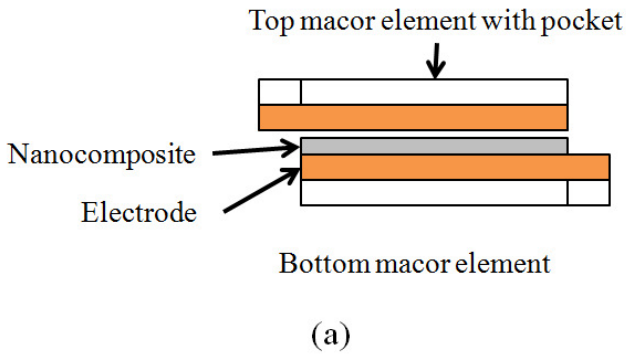

(a)

Macor element electrode post ink print

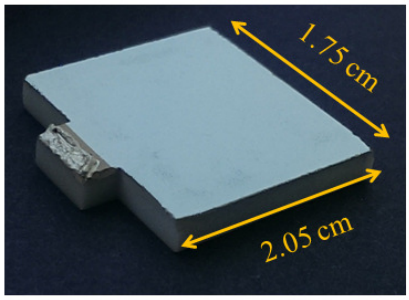

(b)

Figure 1. (a) A schematic diagram of the test device. The upper element has a pocket machined into its top for set masses to rest in; (b) the *macor* electrode complete with a printed ink layer (white layer).

A complementary electrode, with the same *macor* substrate and Cr/Cu/Au layers, was placed on top of the ink. The two tiles were brought into alignment to create the touch sensitive test device. Since the entire printed ink area was being compressed, a 2-probe contact setup was chosen to be the most efficient method available, as a 4-probe technique would involve intricate patterning of contacts and wire bonding to the sides of the printed ink layer, which was only 2-5 μm thick.

Scanning electron microscopy (SEM) was used to analyze the physical structure of the printed ink specimens. The as-printed ink surface shown in figure 2 is complex and homogeneous, with

the TiO_2 needles well dispersed through whole ink surface; they tend to clump into groups of two or three needles. The TiO_2 also appear to predominantly lie in the plane of the surface of the ink and are randomly orientated. The TiO_2 nanoparticles are better dispersed between the acicular particles, and these act to prevent excessive clumping of the TiO_2 needles. Voids are also seen. Closer inspection of the surface in figure 3(a) and (b) reveals a thin, discontinuous coating of polymer on both the TiO_2 needles and nanoparticles. The images show that the polymer content of the printed ink is not significant, present as a thin wetting of the nanoparticles. This allows the composite to be loaded with filler particles above the percolation threshold, as it keeps the particles separate and prevents a direct contact percolation network from forming.

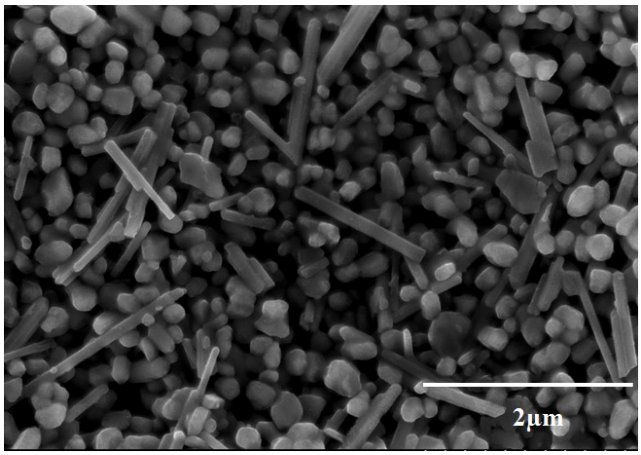

Figure 2. An SEM image of the as-printed ink surface.

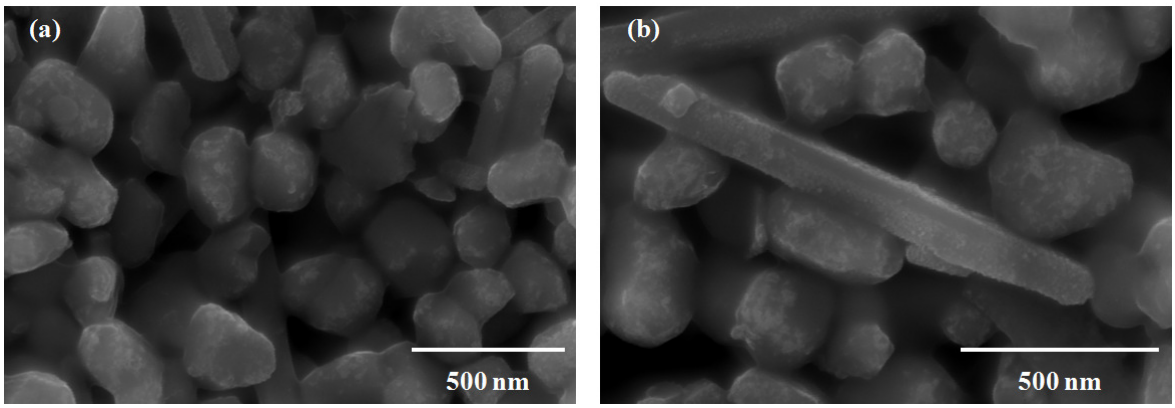

Figure 3. High resolution images of the TiO_2 needles and nanoparticles in the as-printed ink surface.

Focussed ion beam (FIB) milling was employed to etch trenches and expose cross-sections of the printed ink layers, an example of which is given in figure 4. A sacrificial platinum capping layer was deposited by a combination of electron beam- and ion beam-induced deposition to protect the cross-section from undesired wearing and damage by the ion beam during the milling process. As with the top surface structure, the TiO_2 needles are dispersed throughout the whole body of the ink layer, occasionally clumping into groups of 2 to 3 needles. They also tend to lie flat, in the plane of the surface of the ink. The TiO_2 nanoparticles are well dispersed in between the TiO_2 needles, preventing excessive clumping of the needles. The voids seen in the top surface are also present in the ink cross-section. It is believed that these voids lend to the compressibility of the ink.

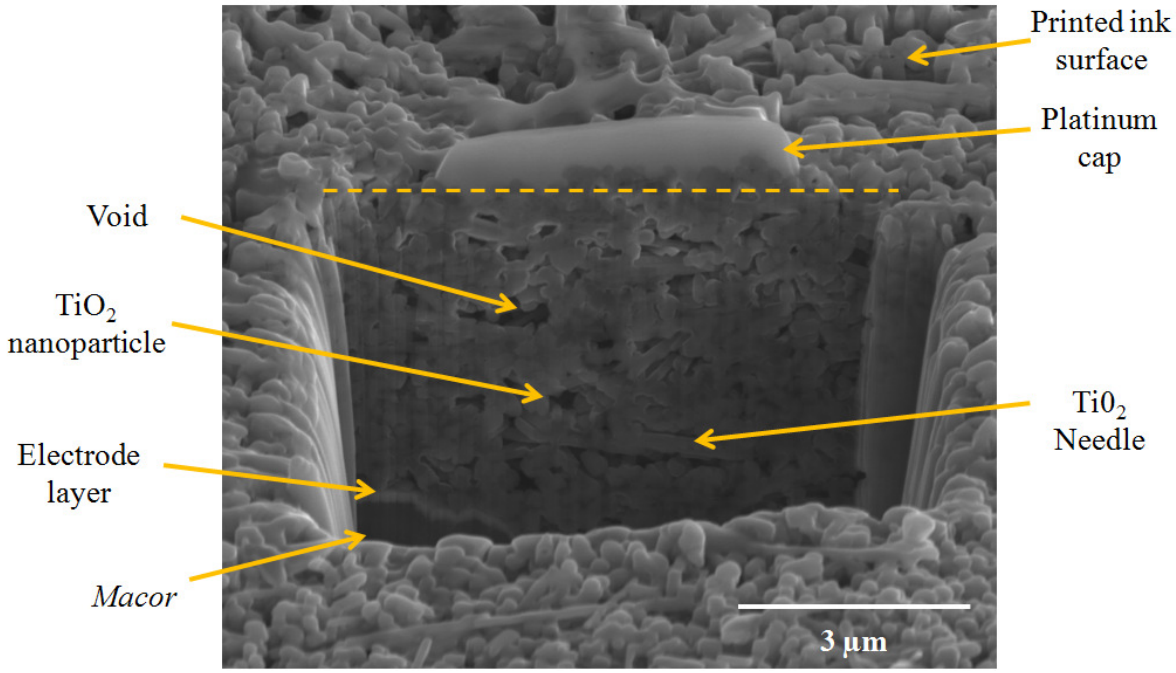

Figure 4. SEM image of an example FIB milled cross-section of an as-printed ink specimen. The dashed yellow line indicates the top of the cross-section trench.

The test device was placed within a compression rig, which was placed inside an oven. The test device was compressed with a series of known mass loads. The entire area of the printed ink specimen (2.05 x 1.75 cm^2) was compressed by the mass load (Here, 1 N is equal to a touch pressure of 2.8 kPa). The compression vector was maintained with the aid of a supporting scaffold.

Previous work[21] has found this ink to be durable and has highly repeatable electrical behaviour even after 1 million compression cycles. Electrical transport behavior was measured as a function of compressive loadings over a range from 0.2 N to 4 N, and temperature ranging from room temperature up to 100 °C. A typical measurement cycle involved loading the device with a selected mass at room temperature and then allowing the device resistance to settle for one hour.

After this time, any creep induced changes of the electrical behavior becomes negligible. The current-voltage (I-V) behavior was measured by ramping voltage from 0 V to 10 V over 5 seconds in 0.1 V steps, and then ramping down to 0 V at the same rate, using a computer controlled Keithley 2420 sourcemeter. For each force and temperature the voltage sweep was repeated ten times. The temperature of the device was increased in increments of 10 °C and the system was allowed to stabilize for 20 minutes before the I-V measurements were taken. This process was repeated up to 100 °C. After cooling to room temperature, the mass loading was increased and the temperature dependence procedure was repeated.

Results and Interpretation

Figure 5 shows examples of the temperature dependence of the I-V behavior of the ink under static compression of 0.6 N. As the temperature increases, the conductivity of the ink increases. This indicates the ink displays a negative temperature coefficient of resistance (NTC) effect. It should also be noted that the I-V also exhibits some limited hysteretic behavior between the up and down sweeps and that this hysteresis has a temperature dependence.

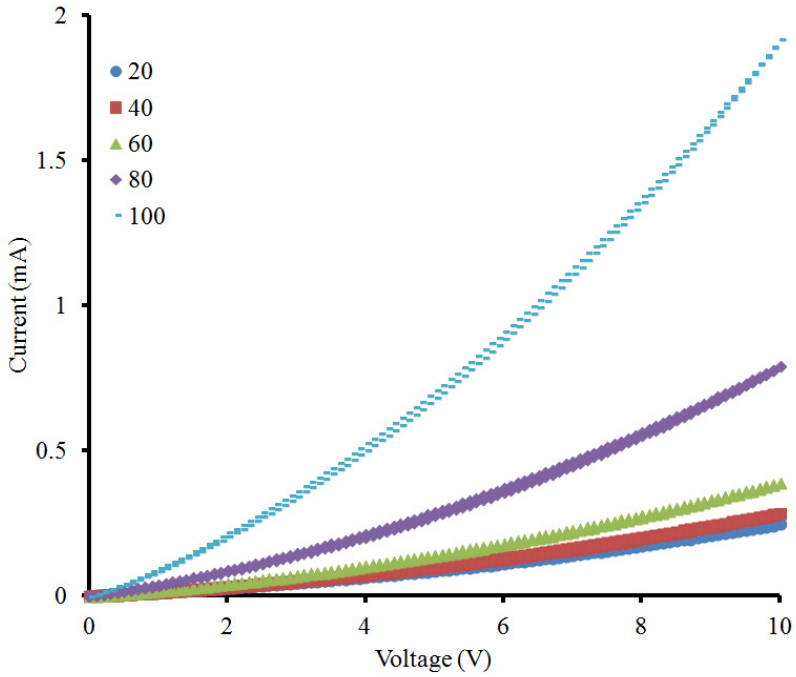

Figure 5. Examples of the I-V behavior of the ink, under a compressive load of 0.6 N, at temperatures from room temperature (20 °C) up to 100 °C.

Details of the hysteresis in the I-V can be observed in figure 6 at 20 °C and 100 °C, for the ink under 0.6 N compression. The hysteresis increases as temperature is increased, albeit slightly. This is indicated by values of δI, the difference between the measured current at a given voltage from the up and down ramps; at 7 V, δI at 20 °C in figure 6(a) is 0.006 mA, whereas δI at 100 °C, figure 6(b) is 0.024 mA. Its presence indicates that the nanocomposite ink has a slightly lower electrical resistance on the ramp down of the voltage during the I-V sweep. The physical basis for this hysteresis and its temperature dependence is currently undetermined. Joule heating and the rate of change of resistance are higher at high compression but the hysteresis is reduced. Charge trapping has been observed to give rise to large hysteresis in Ni elastomer composites[19,20,26] with sample resistances after voltage cycling much smaller than the initial

resistance. This effect is due to charge emission from sharp tips on the Ni particles. A similar, but weaker, effect could occur from the needles in the ink giving much smaller charge trapping and much reduced hysteresis.

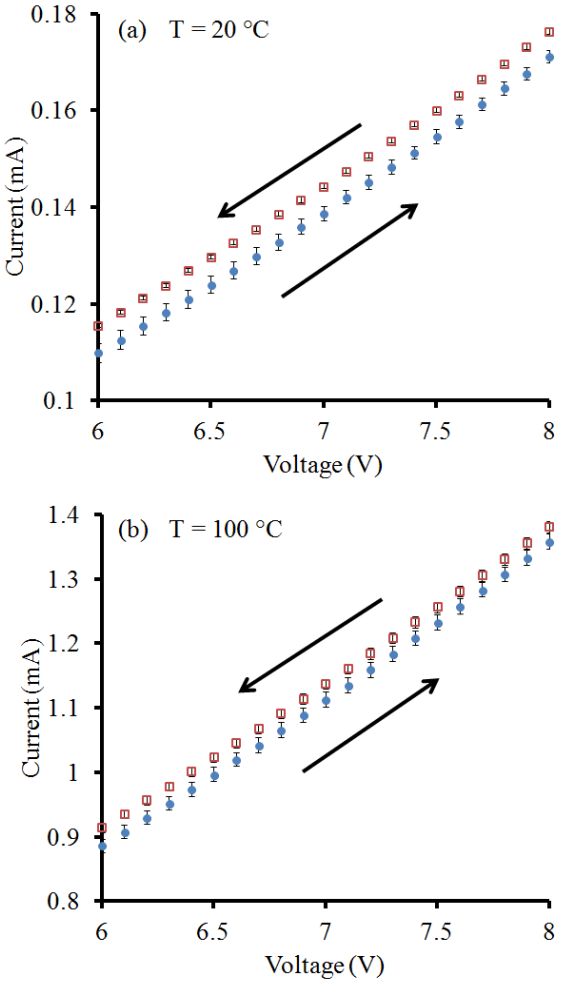

Figure 6. Details of I-V curves for the nanocomposite ink compressed by 0.6 N at temperatures of (a) 20 °C, and (b) 100 °C. The solid circles indicate increasing voltage, while the open squares are data from the decreasing voltage sweep.

In terms of the force dependence, figure 7 shows examples of the I-V data taken at room temperature under compression ranging from 0.2 to 1.0 N. Note that the I-V behavior becomes

more linear with increasing compression, and approximately 100 times more current flows under 0.6 N compression as compared to 0.2 N. Both an increase in temperature and compression act to increase the conductivity of the nanocomposite ink.

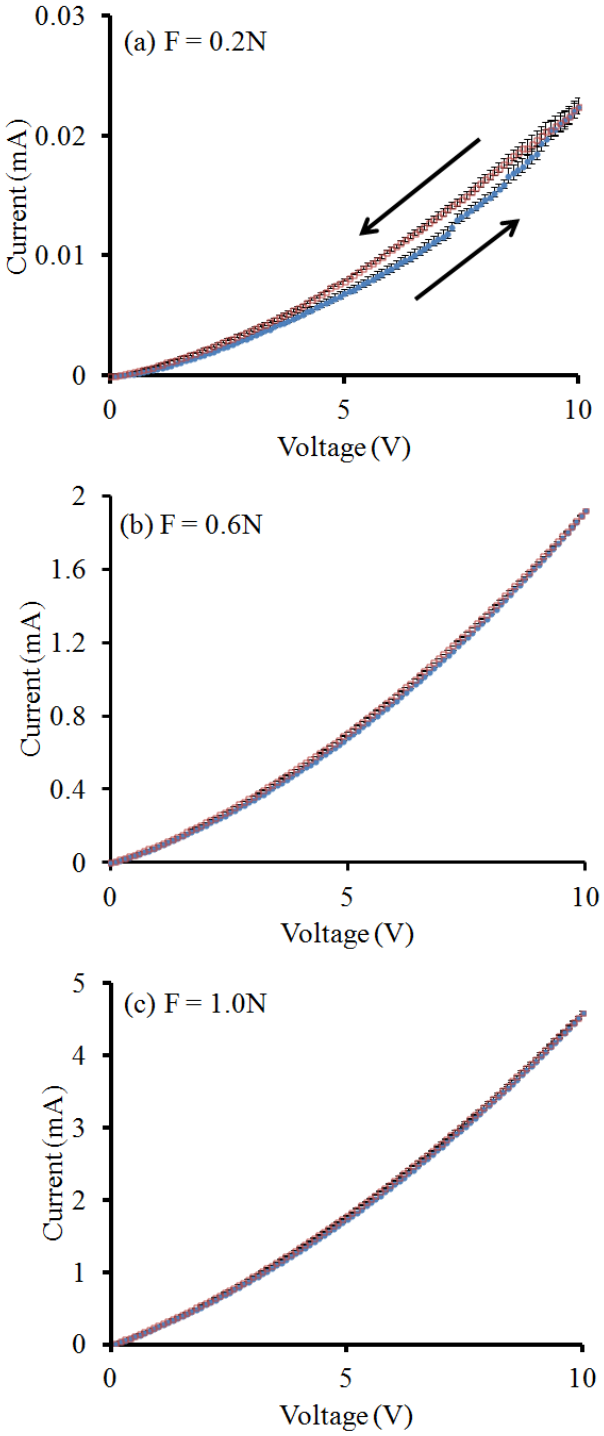

Figure 7. Examples of I-V behavior of the nanocomposite ink at compressive loadings (a) 0.2 N, (b) 0.6 N, and (c) 1 N.

Here, electrical transport data for this nanocomposite ink is interpreted theoretically in terms of a combination of contributions including percolative conduction, that reflects direct contact between conducting filler particles, and a quantum tunneling contribution between isolated filler particles and/or clusters of filler particles. The percolative conduction is represented by a linear ohmic term, and the quantum tunneling contribution is represented by a non-linear constituent, with the total current density equal to the sum of these contributions. This model combination of conduction mechanisms is provided in the relation below[27,28]:

$$J(E)_{TOTAL} = \sigma_0 E + \underline{AE^n exp(-B/E)} \quad (1)$$

Where $J(E)_{TOTAL}$ is the total current density, σ_0 is the linear conductivity, and E is the electric field. The tunneling current density is represented by the underlined exponential function where A is a parameter related to the tunneling frequency or, in other words, the magnitude of tunneling conduction (and contains several correction factors), n is an integer which can take a value between 1 and 3, depending on the details of the internal field emission (for example, $n = 2$ for Fowler-Nordheim tunneling), and B is a constant attributed to the potential barrier height. Field-assisted tunneling is expected to have a specific temperature dependence, which is encapsulated into the temperature dependence of parameter A, according to[29]:

$$A = D(\alpha T/sin\alpha T) \quad (2)$$

where α is a constant, T is the temperature, and D is a parameter comprising all the correction factors and constants found in the parameter A from equation (1).This theoretical model has been used to interpret the experimental I-V sweeps measured for the nanocomposite ink.

Examples of the fitting of equation (1) to the I-V data are shown in Figure 8. Statistical analysis of the fitting was undertaken and normalized residuals are also shown in figure 8. Here, the residuals are obtained as the difference between the experimental data and the best theoretical fits, divided by the errors on the experimental data and plotted against the voltage. A good fit should have randomly scattered residuals and these normalized values should lie between 2 and -2. The analysis indicates that the composite conductivity model is a reasonable description of the transport behavior over much of the electric field range, but a poorer description of the transport behavior in the low voltage region at low compression and low temperature. We see that the model does not produce sufficient current to match observations, so it is likely another form of electrical transport has been overlooked. For example, the test device may be acting as a leaky capacitor, whereby charge accumulates at the electrodes and leaks through the nanocomposite ink. At high temperature and compression, all of the residuals lie between ± 2. This suggests that the model provides a reasonable physical basis to understand the pressure and temperature sensitive electrical transport in such complex nanocomposites.

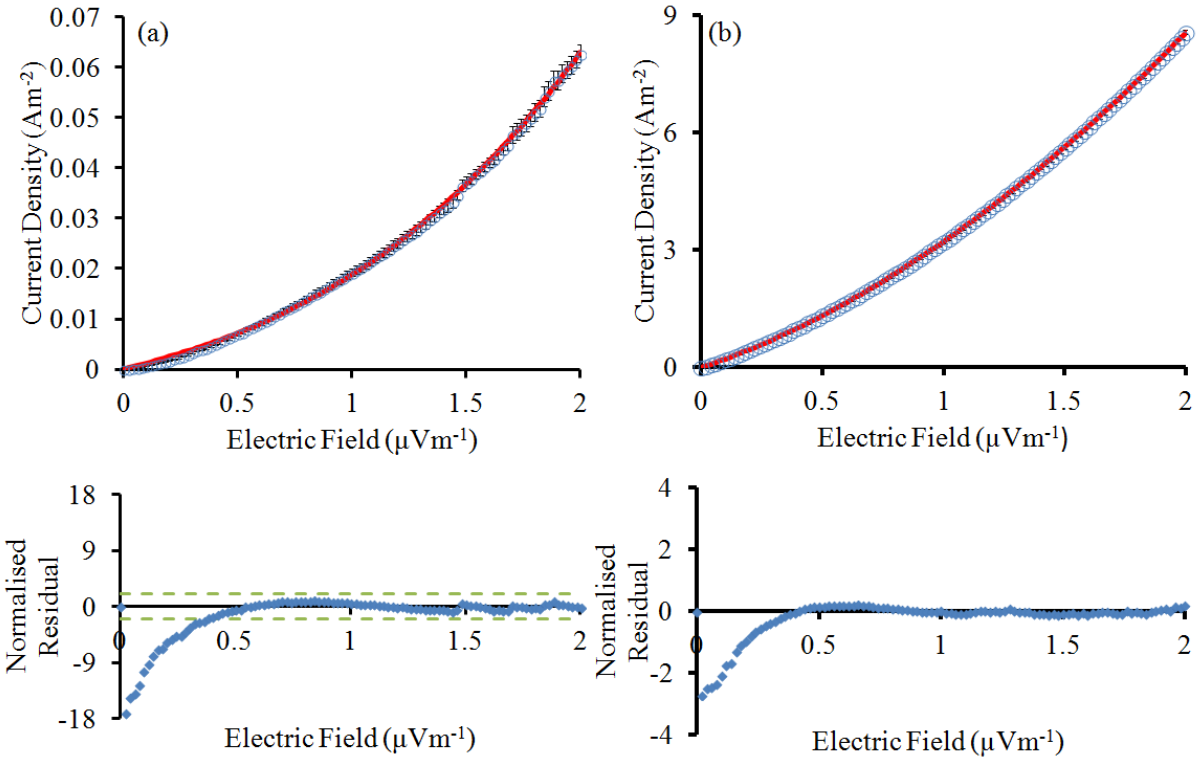

Figure 8. Best fitting theoretical curves (solid line) to measured I-V data (open circles) for (a) 0.2 N compression and at 20 °C, (b) 0.6 N compression and at 100 °C. The normalized residuals are plotted below. The dashed lines show the ± 2 boundaries representing a good statistical fit. Error bars are smaller than the data points.

From the fitting of equation (1) to the I-V data, values for the linear conductivity σ_0 contribution, the non-linear contribution parameter A, and the tunneling exponent n were extracted. Figure 9 shows how these linear and non–linear contributions, and the exponent n vary with increasing compression, at five fixed temperatures. The errors on the linear parameter are relatively large at low forces and at high temperature; nonetheless, the data show that, with increasing compression, the linear contribution to conductivity, (σ_0) increases with increasing loading and tends towards a maximum value by 4 N. The linear conductivity is greater at higher

temperatures. The non-linear contribution A rises at an increasing rate with higher compressive load. The rapid increase of A with compression is also more pronounced at higher temperatures. The errors on the non-linear component are generally small at low and high compressions, becoming larger with increasing temperature. The tunneling exponent n, at room temperature, initially falls from close to 3 to approximately 2 by 1 N compression, remaining close to 2 but gently increasing in magnitude as the compression is increased. As the temperature is increased, the initial value of n at the lowest compression decreases until, by 60 °C, the exponent takes a value of approximately 2 for all but the highest compressions. At and above 60 °C, and at compressions greater than 3 N, the value of n begins to decrease.

The temperature dependence of σ_0 and A are shown in Figure 10, for five compressive loadings. Both σ_0 and A follow a similar temperature dependence, rising at an increasing rate with increasing temperature.

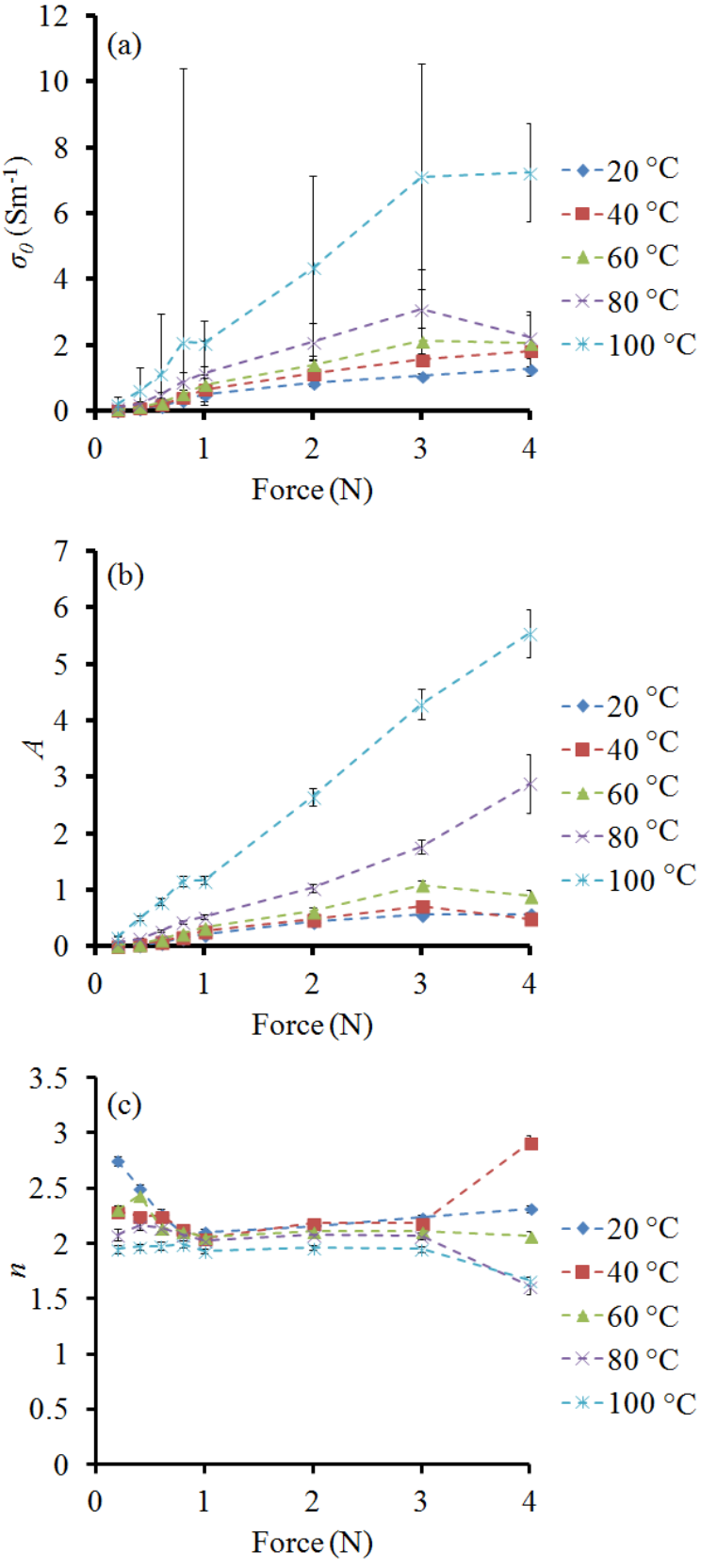
(a)
σ_0 (Sm^{-1})
Force (N)
20 °C
40 °C
60 °C
80 °C
100 °C
(b)
A
Force (N)
20 °C
40 °C
60 °C
80 °C
100 °C
(c)
n
Force (N)
20 °C
40 °C
60 °C
80 °C
100 °C

Figure 9. The variation of (a) the linear conduction parameter σ_0, (b) the non-linear conduction parameter A, and (c) the tunneling exponent n as a function of compressive force. Values for the parameters are shown for 5 temperatures: 20, 40, 60, 80 and 100 °C. The dashed lines are guides to the eye.

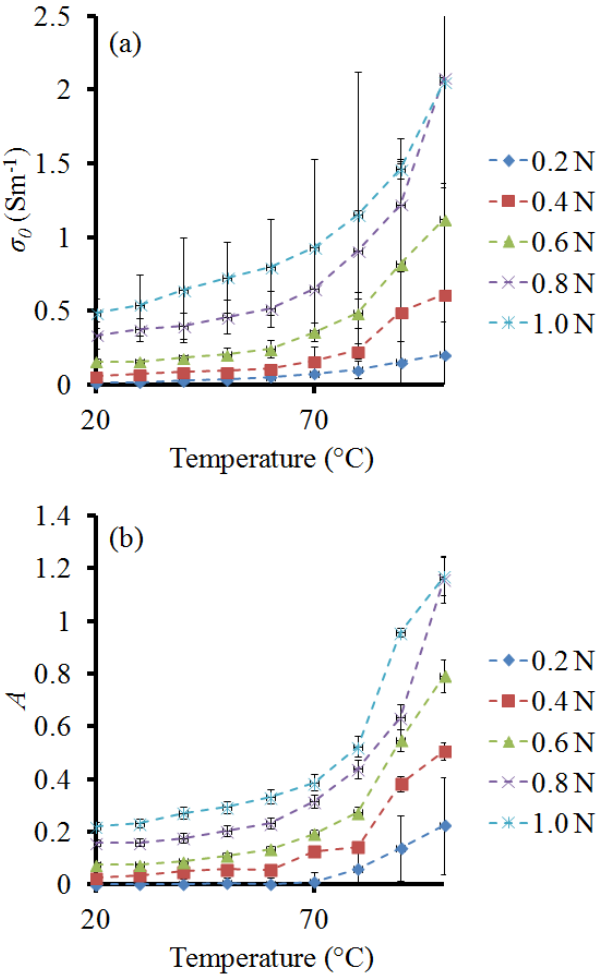

Figure 10. The response of (a) the linear conduction parameter σ_0, and (b) the non-linear connduction parameter A (b), to increasing temperature. Values for both parameters are provided from 5 static compressive loads: 0.2, 0.4, 0.6, 0.8 and 1.0 N. The dashed lines are guides to the eye.

The relative contributions of the linear and non-linear parameters to the overall conduction are shown in Figure 11. We see in figure 11(a), (b), and (c), with increasing temperature at fixed compressions the relative contribution of the linear conduction component falls, while the contribution from the non-linear conduction increases. This is most noticeable at low compressions, and the contributions from both linear and non-linear components vary less with temperature at higher compressions.

At fixed temperatures similar fluctuations in the relative linear and non-linear conductivity contributions are observed with increasing compression with the linear component decreasing and the non-linear component increasing, toward minimum/maximum values. This behavior is reversed at the highest temperature, where the linear conductivity contribution actually increases with compression, with a decrease of the non-linear contribution observed. This suggests that at the highest temperature, increasing compression has a limited effect on the non-linear conduction because it has already reached its maximum and so only the linear contribution increases.

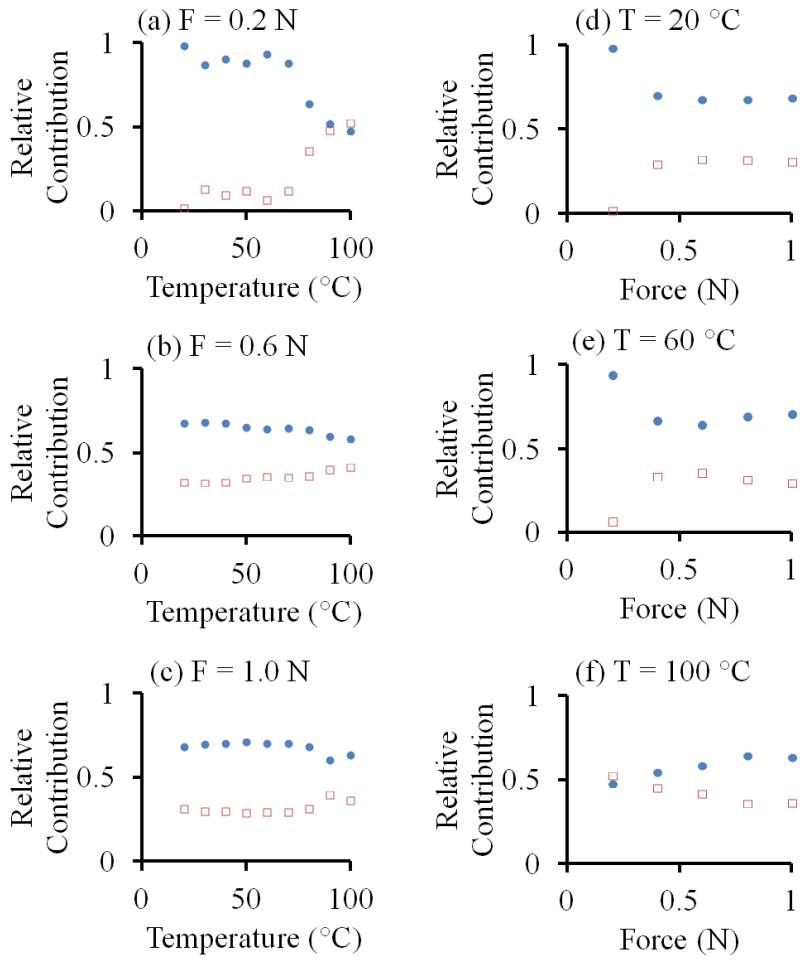

Figure 11. Relative contributions of the linear (solid circles) and non-linear (open squares) conductivity components at fixed compressions of (a) 0.2 N, (b) 0.6 N, (c) 1.0 N, and at fixed temperatures of (d) 20 °C, (e) 60 °C, and (f) 100 °C.

Considering now the conduction mechanisms, the linear conductivity increases with increasing compression and temperature. This suggests some increase in direct connections that enhance percolative conductance. Regarding compression, the applied force brings together the conducting components, establishing more direct connections until no further increase in contact occurs and the conductance reaches a maximum. With increasing temperature the linear

conductance increases more rapidly at higher temperatures. This may be explained by two effects. Firstly, increasing the temperature results in physical softening of the binder; this may aid compressibility and facilitate easier formation of percolative connections. The as-printed binder is quite rigid at room temperature, and its rigidity has not been studied as a function of temperature, so this effect may or may not be significant. Secondly, the intrinsic electrical conductivity of the semi-conducting needles will increase with temperature.

The non-linear conductivity component also increases with compression, and is seen to tend toward a maximum value. As the force on the as-printed ink is increased, the conducting components are forced into closer proximity, narrowing tunneling barriers. This effect is limited by the number of tunneling barriers destroyed as direct connections form between the conducting needles. The non-linear conductivity rises with increasing temperature. An increase in the temperature would provide an additional energy input at tunneling barriers, increasing the tunneling frequency and thus increasing the non-linear conductivity component.

The temperature dependence for the tunneling conduction is captured by equation (2). This was fitted to the experimentally derived non-linear conduction parameter, A, as a function of temperature as shown in Figure 12. The fit is poor at low compression, but improves with increasing compression. The low compression behavior is complicated by the initial contacting between the ink and the top electrode. Beyond this initial contacting, the behavior is more stable and there is reasonable agreement between the data and this theoretical model. This suggests that a field-assisted quantum tunneling component may be appropriate to explain the non-linear component of the electrical conductivity of this nanocomposite ink.

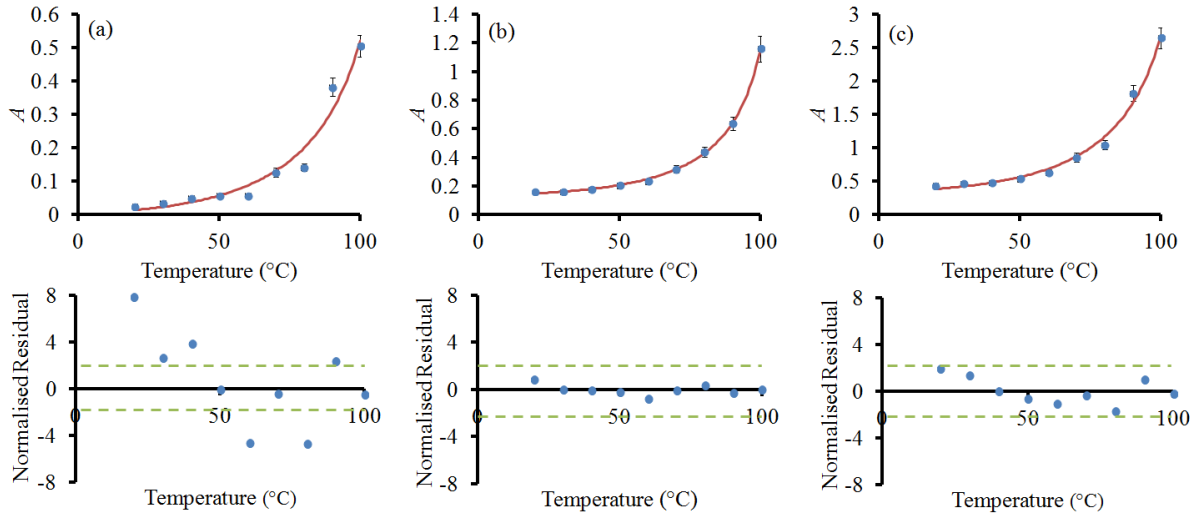

Figure 12. Example fits of the theoretical field emission temperature dependence (solid line) to the calculated values of parameter *A* against temperature at (a) 0.4 N, (b) 0.8 N and (c) 2 N compression, complete with their respective normalized residuals. The dashed lines are a guide to the limits of an acceptable fit in the residual plots.

Conclusions.

In conclusion, the electrical transport behavior of a nanocomposite ink has been studied through measurements of I-V curves taken as a function of static compression and through a range of temperatures. The I-V data are non-linear, and the non-linearity becomes more pronounced as the temperature increases. A small degree of electrical hysteresis is present, but the exact cause of this phenomenon is as yet undetermined. The behavior of this structurally complex composite may be plausibly represented by a model of two competing conductions mechanisms: linear percolative electrical conduction, and a non-linear electrical conduction associated with field-enhanced tunneling between isolated TiO_2 needles and clusters of needles, separated by compressible voids and/or polymer binder wetting. Both of these conduction mechanisms are

sensitive to temperature and together contribute to a negative temperature coefficient of resistance. The theoretical temperature dependence of internal field emission agrees well with the temperature dependence of the non-linear conductivity at low compressions.

AUTHOR INFORMATION

Corresponding Author

*Del Atkinson

e-mail: del.atkinson@durham.ac.uk

Phone: +44(0) 191 33 43529

Author Contributions

The manuscript was written through contributions of all authors. All authors have given approval to the final version of the manuscript.

Funding Sources

This work was funded by the EPSRC.

ACKNOWLEDGMENT

Thanks go to all those at Peratech, notably David Lussey and Paul Laughlin. Thanks also go to Adam Graham for early input into the materials development and sample preparation.

REFERENCES

1. Norman, R. H. *Conductive Rubber: Its Production, Application and Test Methods*, 1st Ed; Maclaren & Sons: London, 1957.

2. Kerner, E. H. The Electrical Conductivity of Composite Media. *Proc. Phys. Soc., London, Sect. B.* **1956**, 69, 802.

3. Bulgin D. Electrically Conductive Rubber. *Rubber Chem. Technol.* **1946**, 19, 667-695.

4. Lu, J.; Weng, W.; Chen, X.; Wu, D.; Wu, C.; Chen, G. Piezoresistive Materials from Directed Shear-Induced Assemply of Graphite Nanosheets in Polyethylene. *Adv. Func. Mater.* **2005**, 15, 1358-1363.

5. Grzelczak, M.; Pérez-Juste, J.; Mulvaney, P.; Liz-Marzán, L. Shape Control in Gold Nanoparticle Synthesis. *Chem. Soc. Rev.* **2008**, 37, 1783-1791.

6. Mionić, M.; Pataky, K.; Gaal, R.; Magrez, A.; Brugger, J.; Forró, L. Carbon nanotubes-SU8 Composite For Flexible Conductive Inkjet Printable Applications. *J. Mater. Chem.* **2012**, 22, 14030.

7. Torrisi, F.; Hasan, T.; Wu, W.; Sun, Z.; Lombardo, A.; Kulmala, T. S.; Hsieh, G-W.; Jung, S.; Bonaccorso, F.; Paul, P. J.; Chu, D.; Ferrari, A. Inkjet Printed Graphene Electronics. *ACS Nano.* **2012**, 6, 2992-3006.

8. Sun, X.; Sun, H.; Li, H.; Peng, H. Developing Polymer Composite Materials: Carbon Nanotubes or Graphene? *Adv. Mater.* **2013**, 25, 5153-5176.

9. Battacharya, S. K.; Chaklader, A. C. D. Review on Metal Filled Plastics .1. Electrical-Conductivity. *Polym. -Plast. Technol. Eng.* **1982**, 19, 21-51.

10. Chawla, K. K. *Composite Materials: Science and Engineering*, Springer: New York, 2012, pp 80-90.

11. Lim, S.; Kang, B.; Kwak, D.; Lee, W. H.; Lim, J. A.; Cho, K. Inkjet Printed Reduced Graphene Oxide/ Poly(Vinyl Alcohol) Composite Electrodes for Flexible Transparent Organic Field-Effect Transistors. *J. Phys. Chem. C.* **2012**, 116, 7520-7525.

12. Chen, B.; Wu, K.; Yao, W. Conductivity of Carbon Fiber Reinforced Cement-Based Composites. *Cem. Concr. Compos.* **2004**, 26, 291-297.

13. Bunde, A.; Dieterich, W. Percolation in Composites. *J. Electroceram.* **2000**, 5, 81-92.

14. McLachlan, D. S. Analytical Functions for the DC and AC Conductivity of Conductor-Insulator Composites. *J. Electroceram.* **2000**, 5, 93-110.

15. Strümpler, R.; Glatz-Reichenbach, J. Conducting Polymer Composites. *J. Electroceram.* **1999**, 3, 329-346.

16. Dai, K.; Xu, X-B.; Li, Z-M. Electrically Conductive Carbon Black (CB) Filled In Situ Microfibrillar Poly(Ethylene Terephthalate) (PET)/Polyethylene (PE) Composite with a Selective CB Distribution. *Polymer.* **2006**, 48, 849-859.

17. Balberg, I. Tunneling and Nonuniversal Conductivity in Composite Materials. *Phys. Rev. Lett.* **1987**, 59, 1305-1308.

18. Balberg, I. A Comprehensive Picture of the Electrical Phenomena in Carbon Black-Polymer Composites. *Carbon.* **2002**, 40, 139-143.

19. Bloor, D.; Donnelly, K.; Hands, P. J.; Laughlin, P.; Lussey, D. A Metal-Polymer Composite with Unusual Properties. *J. Phys. D: Appl. Phys.* **2005**, 38, 2851-2860.

20. Stassi, S.; Canavese, G. Spiky Nanostructured Metal Particles as Filler of Polymeric Composites Showing Tunable Electrical Conductivity. *J. Polym. Sci., Part B: Polym. Phys.* **2012**, 50, 984-992.

21. Webb, A. J.; Szablewski, M.; Bloor, D.; Atkinson, D.; Graham, A.; Laughlin, P.; Lussey, D. A Multi-Component Nanocomposite Screen-Printed Ink with Non-Linear Touch Sensitive Electrical Conductivity. *Nanotechnology.* **2013**, 24, 165501.

22. Lussey, D.; Bloor, D.; Laughlin, P.; Graham, A.; Hilsum, C. (Peratech Ltd.). Electrically Responsive Composite Material for Transducers. UK Patent GB 2462920, March 03, 2010.

23. Gruber, R. (Kronos International, Inc.). Method for Manufacturing Titanium Dioxide. US Patent US20130058860 A1, March 07, 2013.

24. Juergens, V.; Breyder, A.; Mersch, F.; Bluemel, S.; Schmitt, V. (Kronos International, Inc.). Method for the Surface Treatment of Inorganic Pigment Particles. US Patent US20140000483 A1, January 02, 2014.

25. Okuda, H.; Takahashi, H.; Yamada, E. (Ishihara Sangyo Kaisha, Ltd.) Acicular Titanium Dioxide Particles and Method of the Production Thereof. EU Patent EP0341703 A2, November 15, 1989.

26. Bloor, D.; Graham, A.; Williams, E. J.; Laughlin, P. J.; Lussey, D. Metal-Polymer Composite With Nanostructured Filler Particles and Amplified Physical Properties. *Appl. Phys. Lett.* **2006**, 88, 102103.

27. He, L.; Tjong, S-C. Non-Linear Electrical Conduction in Percolating Systems Induced by Internal Field Emission. *Synth. Met.* **2011**, 161, 540-543.

28. He, L.; Tjong, S-C. Universality of Zener Tunneling in Carbon/Polymer Composites. *Synth. Met.* **2012**, 161, 2647-2650.

29. Murphy, E. L.; Good, R. H. Thermionic Emission, Field Emission, and the Transition Region. *Phys. Rev.* **1956**, 102, 1464-1472.